Expression of Interest for an Experiment Searching for μ-e Conversion at J-PARC Muon Facility

M. Kinsho,
JAERI, Tokai, Ibaraki, Japan

M. Ikegami, S. Mihara, H. Nishiguchi, C. Ohomori, M. Yoshii
KEK, Tsukuba, Ibaraki, Japan

M. Aoki*
Osaka University, Toyonaka, Osaka, Japan

T. Numao
TRIUMF, Vancouver, BC, Canaka

D. Bryman
the University of British Columbia, Vancouver, BC, Canaka

January 8, 2010

*Contact Person

Abstract

A new experiment searching for μ-e conversion by fully utilizing the high-power pulsed proton beam available at J-PARC MLF will be discussed. Both a Monte Carlo simulation and a test measurement indicated that the muonic carbon atom formation rate in a muon target of MLF J-PARC is approximately 10^{10}/sec for 1 MW operation of the RCS. With this high formation rate of the muonic atoms, it is possible to perform a competitive search for μ-e conversion from the muon production target itself at the level of 10^{-14}, nearly two orders of magnitude below current limits. A new secondary beam line at the High-Momentum Decay Muon port will be dedicated to extract 105-MeV/c electrons from a muon stopper placed near the muon production target. A high performance kicker system is used in the secondary beam line to eliminate the prompt beam burst. This beam line can be upgraded to a high-momentum decay muon beam line after the completion of the μ-e conversion experiment.

Table 1: Present limits on CLFV from muon experiments.

Reaction	Present limit	Reference
$\mu^+ \to e^+\gamma$	$< 1.2 \times 10^{-11}$	[3]
$\mu^+ \to e^+e^+e^-$	$< 1.0 \times 10^{-12}$	[4]
$\mu^- + \mathrm{Ti} \to e^- + \mathrm{Ti}$	$< 6.1 \times 10^{-13}$	[5]
$\mu^- + \mathrm{Au} \to e^- + \mathrm{Au}$	$< 7 \times 10^{-13}$	[6]

1 Introduction

Lepton flavor invariance, which was a feature of the original Standard Model (SM) *a priori*, no longer holds since observations of neutrino oscillations have been firmly established[1]. This fact generally implies the existence of lepton flavor violation in charged sector (CLFV) due to the mixing of neutrino flavors in the intermediate state, but the strength of such a process is suppressed by a GIM-like mechanism to the level of 10^{-60}[2] far beyond experimentally accessibility. Since CLFV is practically still forbidden in the framework of neutrino-oscillation-extended SM, the experimental observation of CLFV would signal the existence of extraordinary new physics beyond the Standard Model.

While experimental searches for CLFV processes have been performed using many processes such as muon decays and reactions, tau decays, kaon decays, etc, muons provide the highest sensitivity. Table 1 shows the current limits on CLFV from several muon experiments. The reason why muons are suited for CLFV search experiments can be naively explained by two features: higher muon production rate and the long muon life time. A leading new experiment searching for $\mu^+ \to e^+\gamma$ at the level of 10^{-13} is on-going at PSI (MEG). Among possible muon experiments, mu-e conversion i.e. the neutrinoless muon capture reaction $\mu^- + \mathrm{A(N,Z)} \to e^- + \mathrm{A(N,Z)}$ is highly favorable for future study since a wide range of new models involving both quark and lepton processes may contribute. Mu-e conversion is experimentally advantageous because the signature involves a single mono-energetic electron for which backgrounds are low and which does not suffer from random coincidence backgrounds as in the case of $\mu^+ \to e^+\gamma$. Two major new experimental enterprises aiming to search for $\mu^- + \mathrm{Al} \to e^- + \mathrm{Al}$ at a level of 10^{-16} have been proposed at JPARC (COMET) and Fermilab (Mu2e). While these may take a decade to mount and operate and require extraordinary financial and technical investments, an opportunity exists at the JPARC MLF to reach the level of 10^{-14}, two orders of magnitude below current limits, with modest cost and a near-term time scale.

Numerous theoretical models give predictions for the branching ratios of CLFV processes[7, 8, 9]. One such model, for example, is based on the combination of a supersymmetric model (SUSY) with a see-saw mechanism by right-handed heavy neutrino[10]. An interesting mass range of the right-handed heavy neutrino could be explored by CLFV experiments such as $\mu \to e\gamma$ and $\mu^- - e^-$ conversion. In addition, experimental studies of these processes are very important to understand the structure

of neutrino sector. Another model based on SUSY Grand Unified Theory[11, 12] also gives predictions for the branching ratio of $\mu \rightarrow e\gamma$ and $\mu^- - e^-$ conversion. In this model, relatively a large top-quark mass results in rather larger radiative corrections to the slepton mass matrix, and the off-diagonal elements of the slepton mass matrix become sizable. As a result, smuon-selectron mixing in the intermediate state of the processes might induce CLFV, and calculations show the branching ratios being only a few orders of magnitude below the current experimental limits.

Despite the theoretical predictions above, no CLFV process has been found yet. That means, new experimental studies of the muon CLFV are presently aiming for fundamental discoveries. Since there are potential differences in the type of interactions mediating $\mu \rightarrow e\gamma$ and $\mu^- - e^-$ conversion, performing searches for both processes (and others) is very important to maximize the discovery potential. Even after the discovery, it will be important to study these processes and others to understand the details of CLFV process.

A CLFV signal may be seen by experiments which improve the current limits and it is conceivable that the CLFV signal lies waiting to be discovered right under the current limit. A new experiment searching for $\mu^- - e^-$ conversion process at the 10^{-14} level would be a highly competitive addition to the field.

2 Overview of Experiment

The new idea of the experiment searching for μ^- + A(N,Z) $\rightarrow$ e^- + A(N,Z) will be described below.

2.1 Muonic Atom Formation in a Muon Production Target

When a high intensity proton beam from the MLF hits a production target, a huge number of pions is copiously produced. The energy distribution of these pions shows a very diverse spectrum ranging from very low energy to high energy, and the production yield of low energy pions is quite large. Some of those low energy pions stop in the production target itself and decay to muons by $\pi^+ \rightarrow \mu^+\nu_\mu$ decays. Since the energy of those decay-at-rest muons is only 4 MeV and the range is not longer than 1 mm in solid material, most of those muons do not emerge from the production target. However, muons from the pions stopped in the very thin surface layer of the production target can emerge from the target. This is the mechanism of how "surface muons" are produced. Since the yield of low energy pions is very large, the yield of surface muons is also large. For example, the typical yield is about 10^8/sec at the PSI πE5 beamline (150 msr, $\Delta p/p = 10\%$).

The probability of 4 MeV muons getting out of the muon target in MLF J-PARC is calculated to be only a level of 10^{-3}[13]. Assuming the acceptance of typical beamline to be 10^{-2}, the number of μ^+ stopped in the production target should be a level of 10^{13}/sec or more.

It is well known that the "surface μ^-" does not exist because the parent particle π^- is promptly absorbed by the target nucleus after it stops and does not decay.

However, low energy pions moving near the target will decay and produce low energy μ^-s. These muons are called "cloud μ^-", and it is known by experience that the yield of cloud μ^- is about 2% of the surface μ^+ when observed by a typical beam line.

Some fraction of the low energy cloud μ^- produced around the target stops in the target or material placed near the target. Then, those μ^- will from muonic atoms. By taking into account the μ^+ stopping rate ($\sim 10^{13}$/sec), the ratio of cloud-μ^- to surface-μ^+ ($\sim$2%), and material near the target, the yield of muonic atom formation at a level of 10^{10}/sec, can be estimated (see below).

2.2 μ-e Electrons from the Muon Production Target

Once muonic atoms are formed in the production target or the material near the target, one of following processes will occur:

1. Muon decay in orbit (DIO): $\mu^- \to e^- \nu_\mu \overline{\nu}_e$,
2. Muon capture (MC): $\mu^- + \mathrm{A(N,Z)} \to \nu_\mu + \mathrm{A'(N,Z\text{-}1)}$ or
3. μ-e conversion (MEC): $\mu^- + \mathrm{A(N,Z)} \to e^- + \mathrm{A(N,Z)}$.

The former two processes are well described within the SM, but the last process, MEC, is a CLFV process that the experiment described here is searching for. Both DIO and MEC processes emit electrons. The electron from MEC is mono-energetic at E_{max}, where E_{max} is given as:

$$E_\mu = E_{\mathrm{max}} + \frac{E_{\mathrm{max}}^2}{2M_A}\,, \tag{1}$$

$$E_\mu = m_\mu - B_\mu\,. \tag{2}$$

M_A is the mass of the target nucleus, m_μ is a mass of muon and B_μ is a binding energy of μ^- in the Coulomb potential of the muonic atomic. Since the B_μ of $^{12}_{6}$C is 0.101 MeV and that of $^{27}_{13}$Al is 0.463 MeV[14], E_{max} is 105.1 MeV and 105.0 MeV for $^{12}_{6}$C and $^{27}_{13}$Al, respectively. On the other hand, the electron energy from DIO shows continuous spectrum from 0 MeV to E_{max}, and the spectrum falls steeply above $m_\mu/2$. Figure 1 shows the energy spectrum of DIO from muon decays in orbit for Aluminum. The spectrum shape near E_{max} is very steep and known to be approximated by $(E_{\mathrm{max}} - E_e)^5$. Therefore, the contamination of DIO electrons to signal electrons can be suppressed by raising the lower energy threshold for the signal electron detection.

The second feature of MEC electron is its timing. Since MEC electrons are emitted by μ^- bound in material, they show an exponential time spectrum, $e^{-t/\tau}$, where τ is a μ^- lifetime in the material. Since μ^-s disappear through DIO and MC, the lifetime becomes shorter than the life time in free space where MC does not happen. The μ^- lifetime in carbon is 2.03 μsec, and that in Aluminum is 0.88 μsec. It is noteworthy that they are indeed shorter than the lifetime in free space but still longer than the time scale of electromagnetic and strong interactions.

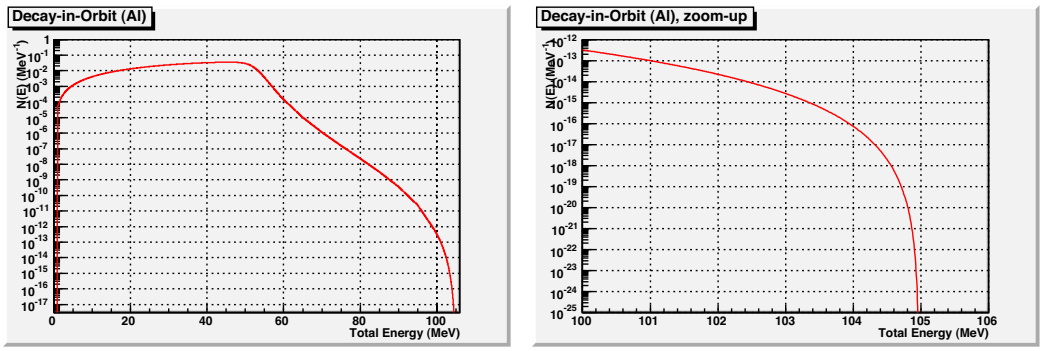

Figure 1: Total energy spectrum of electrons from muon decays in orbit for Aluminum.

There are potential sources of 105-MeV electrons from the production target, but almost all of them are from either electromagnetic interactions or strong interactions followed by electromagnetic interactions. One example is $\pi^0 \rightarrow \gamma\gamma$ followed by γ converting to e^-e^+. Those electrons are emitted without any delay after proton hitting the target. This contrasts with the delayed emission of electrons from μ^- in material. Actually, the source of the delayed electrons whose time scale is the order of the muon life time is only from muon decay. Because of this, if there is any electron emission with energy $E_{\rm max}$ delayed by μsec order after proton hitting the target, it is a signal of MEC.

The potential source of background may be from off-timing protons hitting the production target. In order to suppress those kind of backgrounds, the off-timing protons should be suppressed as less as 10^{-14} of on-timing protons.

2.3 Detection of μ-e Electrons

The μ-e electrons produced in the muon production target can be extracted by a secondary beamline. This secondary beamline should have the following functions:

1. Capability of extracting high momentum 105-MeV electrons;
2. Large solid angle to increase the physics sensitivity;
3. Modest momentum bite to suppress DIO electrons; and
4. Pulse kicker system to eliminate the prompt burst.

The model of the beam line above is the existing beam line at MLF Muon Facility, D2. It can be operated up to 120 MeV/c, which satisfies the 1st requirement above, and the geometrical acceptance is about 40 msr. Three dipole magnets almost completely eliminate low momentum particles passing through the beam line, and the pulse kicker would be used.

Although it is possible to perform the experiment at D2, the sensitivity is limited since it is limited by the solid angle, beam transmission and beam availability. Since it is critically important to increase the acceptance of beamline a new beamline using

the High-Momentum Decay Muon port is very attractive. The physics sensitivity at the new beam line could be more than an order of magnitude better than the measurement using existing D2 as described in the next section.

The secondary beam coming from the muon target at the prompt timing consists of electrons, muons and pions. The muons will stop in inner walls of vacuum duct as well as slits all along the beam line equipments, and produce DIO electrons at the delayed times, constituting another source of background. If the position of a muon is close to the beam line exit, those DIO electrons will emerge out of the beam line exit. Therefore, the electrons coming out of the beam line are not always 105 MeV/c even if the beamline momentum is set at 105 MeV/c. It is therefore necessary to place a magnetic spectrometer at the exit of the beamline, and measure the electron momentum precisely.

3 Experimental Setup Configurations

There are three potential configurations of the experimental setup according to the size of construction cost and the physics sensitivity. Configuration A would clearly have the maximum impact and should be realized as soon as possible.

Table 2 summarizes these configurations.

Table 2: Comparison of three differenct configurations.

	Configuration		
	A	B	C
Muon Stopper	Al Disk	Al Disk	Muon Target
Beamline	New†	D2	D2
Pulse Kicker	New	Modified	Modified
Beam Time Conflict	no	yes	yes
Physics Sensitivity	$< 10^{-14}$	2×10^{-13}	8×10^{-13}
Cost	Modest	Intermediate	Low

†) at the High-Momentum Decay Muon port.

3.1 Configuration A

In configuration A, a new beamline dedicated for this experiment would be built at the High Momentum Decay Muon port. Figure 2 shows schematic plan view of the proposed beamline. In addition, an Aluminum muon stopper will be installed near the production target. Figure 3 shows one example of how the Aluminum muon stopper could be installed. The distance between the production target and the Aluminum muon stopper should be as close as possible. It should not be larger than a few cm to maintain the muonic Aluminum atom formation rate. The thickness of the muon stopper should be optimized to balance the muonic atom formation rate and the

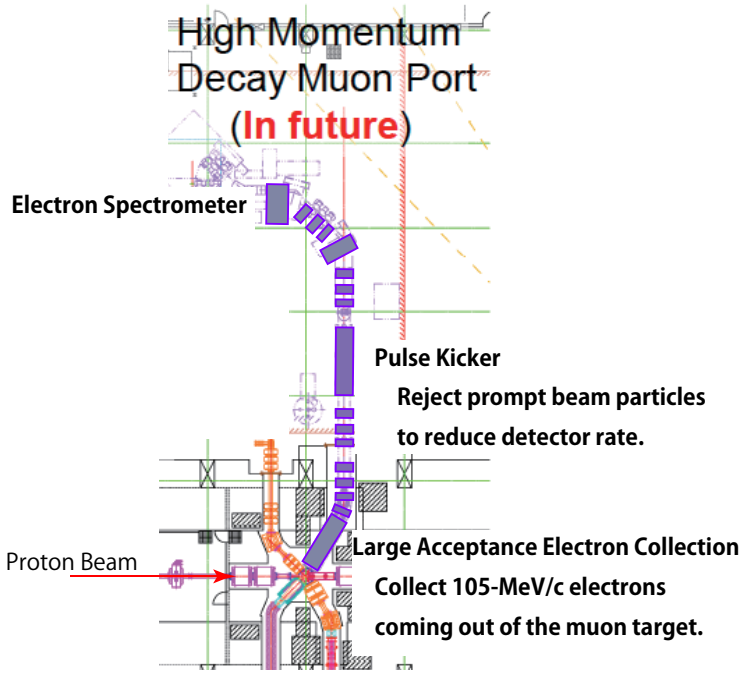

Figure 2: Schematic plan of the Configuration-A with the new beamline placed at the High Momentum Decay Muon Port.

energy loss of the electron in the muon stopper. In the current design, it is chosen to be $1 \sim 3$ mm. The muonic Aluminum atom formation rate in the Aluminum muon stopper is estimated to be 1.5×10^9/sec per 1 mm thickness of the stopper for 1 MW primary proton power. This is only 20% of that in the muon production target itself. However, the muon capture rate is more than 10 times larger in Aluminum than in Carbon.

The configuration A provides the maximum sensitivity compared to the other configurations, and makes it possible to search for μ-e conversion in Aluminum better than BR $< 10^{-14}$, which is almost 2 orders of magnitudes better than the current limit.

The highest sensitivity of the configuration A over the other configurations comes from the following features:

- Larger geometrical acceptance (150 msr) than the existing beamline (40 msr),
- Larger transmission efficiency than the existing beam line,
- No conflict in the beam time with the other experiments,
- Use of the Aluminum muon stopper.

It should be noted that the surface muon yield at the existing beam line would be reduced by factor 2 at most due to the Aluminum muon stopper. However, this

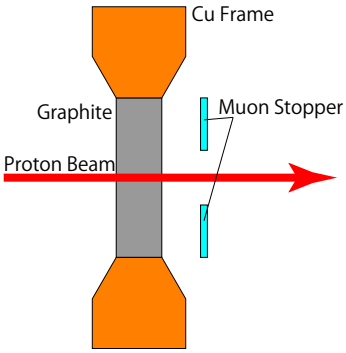

Figure 3: One example of how the Aluminum muon stopper could be installed near the muon target. Please note that the design is not final.

demerit can be automatically solved once the surface muon beamline at the Surface Muon port, which extracts the surface muon to the upstream side of the target, is in operation.

The drawback of the configuration A is its cost since the new beamline is needed. However, it should be stressed that the equipment required for the configuration A can be reused in the construction of the High Momentum Decay Moun beam line. Therefore, the additional cost which is needed only for the configuration A is not substantial.

3.2 Configuration B

In the configuration B, the existing beamline, D2, would be used to extract 105-MeV electrons from the Aluminum muon stopper. The pulse kicker already planned to be installed in the existing beam line may need to be modified so that the flat top of the kicker should be long enough to cover two prompt proton pulses.

The realization of the configuration B would be much faster in schedule and lower in cost than the configuration A. However, the geometrical acceptance is smaller by factor $4 \sim 5$ and the available beam time would be heavily restricted by the conflict with other experiments. The expected physics sensitivity with the configuration B is 2×10^{-13} at most.

3.3 Configuration C

In the configuration C, The Aluminum muon stopper will not be used, and thus μ^- will be captured in Carbon atoms in the muon production target. The modification to the pulse kicker may be still needed. The major drawback is its rather lower physics sensitivity, which is estimated to be at the same level as the current limit.

4 Experimental Apparatus

Although the detailed design of the experimental apparatus depends on which configuration is taken, the overall concept of the experiment is the same. The setup consists of three parts:

- Target section,
- Electron extraction beam line section, and
- Electron spectrometer section.

4.1 Target Section

The function of the target section is three fold:

- Production of π^- from the primary proton beam,
- Letting pions decay to muons, and
- Stoping μ^- in the muon stopping material.

The figure of merit of the target sections can be evaluated by the following formula:

$$\mathrm{FoM} \;=\; R_{\pi^-} \times f_{\pi^- \to \mu^- \mathrm{stop}} \times f_{\mathrm{MC}} \times f_{\mu-e} \times A_{\mu-e}\,, \tag{3}$$

where R_{π^-} is π^- production rate, $f_{\pi^- \to \mu^- \mathrm{stop}}$ is a fraction of π^- that produce μ^- stopped in the muon stopper, f_{MC} is a fraction μ^- that goes to the muon capture process, $f_{\mu-e}$ is the relative strength of the μ-e conversion process, and $A_{\mu-e}$ is the acceptance for 105-MeV/c electrons.

4.1.1 Monte Carlo Estimates

There is no room to optimize R_{π^-} since it is given by the primary beam power and the muon produciton target thickness. R_{π^-} was estimated by using a measured pion production cross section by 2.9 GeV proton on a Be target[15]. Figure 4 shows the pion production cross section used in the calculation. Solid curves in the figure are from an empirical formula as follows:

$$\begin{aligned}\frac{d^2\sigma}{dEd\Omega}&[\mu\mathrm{barn/MeV\cdot sr}] \\ &= \frac{80 \times 40aE}{(33 + 1200a + 40aE)(1 + \exp(40aE/60 - 2))(1 + \exp((E - 1000)/200))}\,,\end{aligned} \tag{4}$$

where

$$a \;=\; 0.001 + 0.02\tan\theta_1\,, \tag{5}$$

$$\theta_1 \;=\; \begin{cases} \dfrac{\theta}{1.5} & (\theta < 90^\circ) \\ 0.32(\theta - 90^\circ) + 60^\circ & (\theta > 90^\circ)\,, \end{cases} \tag{6}$$

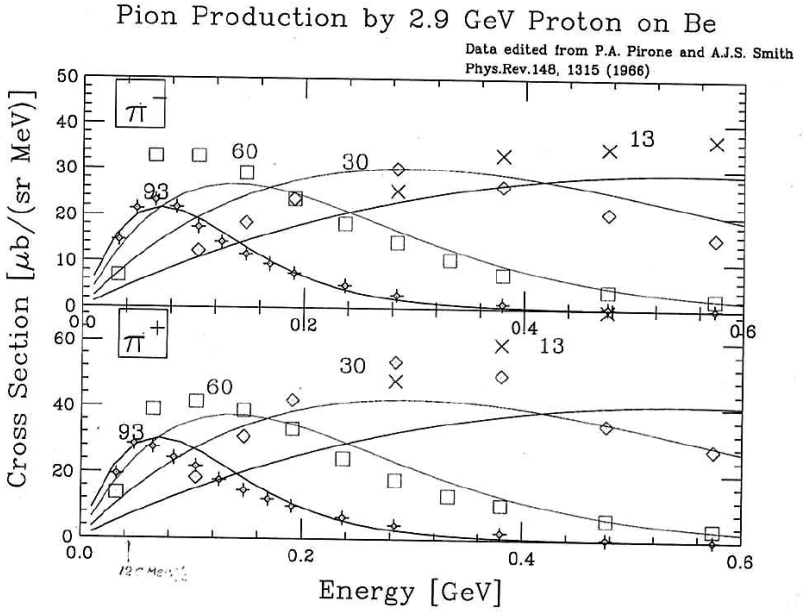

Figure 4: Pion production cross section by 2.9 GeV proton on Be target.

and E is in MeV. This formula was used by Ishida in his surface muon yield calculation[13] for the design of the MLF Muon Facility. By integrating this cross section for all directions and up to 400 MeV/c of pion momentum, the total cross section becomes 50 mb. That means the total pion prodution rate is 2×10^{13} for 1 MW of proton beam on the muon target from RCS.

This pion yield was double checked by using experimental data by HARP[16]. HARP is an experiment measuring charged pion production for various proton energies and materials. The cross sections of pion production by 3 GeV/c–12 GeV/c protons on carbon target are available. The double-differential cross section of π^- production by 3 GeV/c on carbon for $0.95 < \theta < 1.15$ and $0.10\ \mathrm{GeV}/c < p_\pi < 0.15\ \mathrm{GeV}/c$ is

$$\frac{d^2\sigma}{dpd\theta} = 0.038 \pm 0.013\,\mathrm{barn/GeV}/c \cdot \mathrm{rad} \quad (7)$$

Integration over $0.95 < \theta < 1.15$ and $0.10\ \mathrm{GeV}/c < p_\pi < 0.15\ \mathrm{GeV}/c$ gives $\sigma = 0.4 \pm 0.1$ mb. The pion production cross section from Eq. (4) for the same kinetic region is 0.9 mb. They are consistent within factor two.

The factor $f_{\pi^-\to\mu^-\mathrm{stop}}$ is defined by the geometrical configuration of the target section, such as the target thickness, target radius, muon stopper thickness, distance between the muon stopper and the target and its material. A Monte Carlo calculation using Geant4 was performed to estimate $R_{\pi^-} \times f_{\pi^-\to\mu^-\mathrm{stop}}$. The hadron code used for the estimation was QGSP_BERT_HP. The pion production rate of the QGSP_BERT_HP was compared with the HARP result, and showed very good consistency. The results are $R_{\pi^-} \times f_{\pi^-\to\mu^-\mathrm{stop}} = 7\times10^{-9}$/sec for the muon production target for 1 MW operation of the MLF, $R_{\pi^-} \times f_{\pi^-\to\mu^-\mathrm{stop}} = 1.5 \times 10^{-9}$/sec for Aluminum

muon stopper (1 mm thickness).

$f_{\rm MC}$ and $f_{\mu-e}$ are functions of atomic number Z of target material. Table 3 shows $f_{\rm MC}$ and $f_{\mu-e}$ for different materials[17].

Table 3: μ^- capture rate and lifetime for different materials.

	carbon	aluminum	titanium	lead
Atomic Number	6	13	22	82
Capture Rate ($\times 10^6\,{\rm s}^{-1}$)	0.039	0.68	2.6	15
Lifetime (μs)	2.0	0.88	0.33	0.082
$f_{\rm MC}$	0.08	0.60	0.85	0.97
$f_{\mu-e}$[18]	0.7	1	1.7	1.15

$A_{\mu-e}$ is an acceptance to the μ-e electrons. This factor is mutually correlated with the energy spread of the outgoing electron by the energy loss in the target and the momentum acceptance of the secondary beam line as well as the momentum cut required to suppress DIO background. Since the sensitivity goal of this experiment is 10^{-14}, the energy threshold to suppress DIO background would be around 102.5 MeV. This is almost 2.5 MeV below the end point energy, and therefore the event selection efficiency is taken as 100%.

4.1.2 Measurement of Muonic Carbon Atom Formation Rate

The estimation of the muonic carbon atom formation rate described above showed excellent agreement between the two measured cross section data sets (Piroue and HARP) and the QGSP model of Geant4. However, those cross section data do not completely cover whole the kinematical region, and the QGSP model is just a model with some uncertainty in its precision at the low energy region. Therefore, a test experiment to measure the muonic atom formation rate in the Muon Target of MLF was performed in November 2009 (A similar measurement was also performed at TRIUMF in 2008[20]). Figure 5 shows a typical time spectrum of delayed electrons with 40 MeV/c at D2 beamline. The decay constant is consistent with the life time of μ^- bound in the carbon atom. Figure 6 shows the beam line momentum dependence of the delayed electron yield at D2. The shape is quite consistent with the Michel spectrum of bound μ^- with energy loss by 20-mm^t carbon. The beam line transmission of D2 was estimated by G4Beamline with proper fringing field effects for both quad and dipole magnets. The acceptance of the 1st quad triplet section is 40msr which is quite consistent with the geometrical solid angle of the D2 port. The transmission of D2 is a bit worse due to the higher order effects coming from the fringe field of the quadrople magnets, and the overall transmission efficiency for DIO electrons at the 40-MeV/c setting was 6.4×10^{-7} including geometrical acceptance, momentum acceptance and transmission efficiencies. As a result, the rate of the muonic carbon atom formation in the current muon target was obtained to be 8.4×10^8/sec for 110 kW

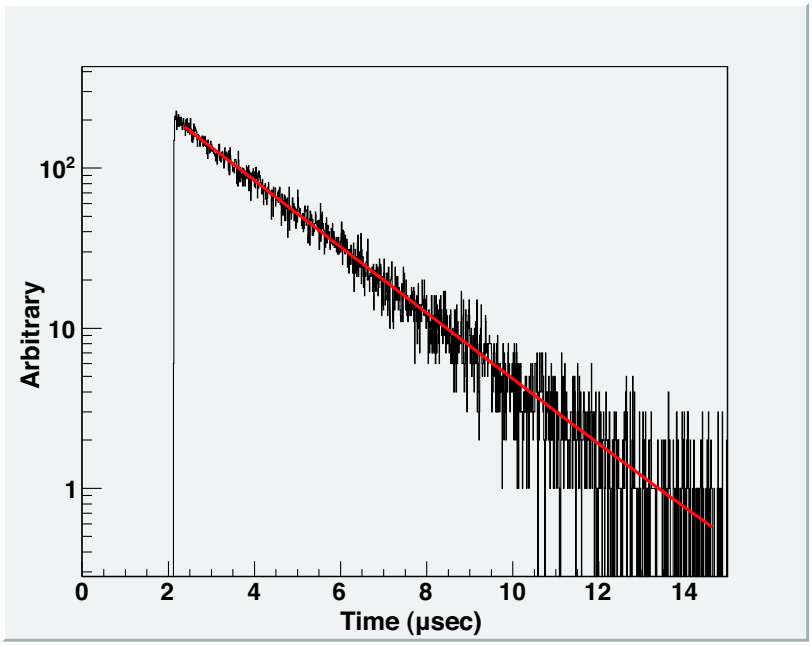

Figure 5: Typical time spectrum observed at the exit of D2 beamline. The origin of horizontal axis is a time of the 1st proton pulse.

operation of MLF. It corresponds to 7.6×10^9/sec for 1 MW operation, and is quite consistent with the estimate obtained by Monte Carlo calculations.

4.2 Electron Extraction Beamline

The secondary beamline is used for extracting μ-e electrons from the muon target to the detector section. It is also required to reject prompt particles so that they do not enter to the detector section blinding the detectors.

4.2.1 Acceptance

The geometrical acceptance of the beam line is a key to achieve the ultimate sensitivity. In the configuration A, it will be almost 150 msr if an axial focusing element is used, while it is only 40 msr for the existing beam line. The transmission efficiency of the existing beam line is also not high due to the fringe field effects of the quadrupole magnets. The overall difference will be more than an order of magnitudes.

The momentum acceptance does not have to be large. It is better to accept electrons with momentum from 100 MeV/c to 107 MeV/c, where 100–102.5 MeV/c is the DIO region, 102.5–105.0 MeV/c is signal region, and 105.0–107.0 MeV/c is a higher momentum region to monitor the prompt background.

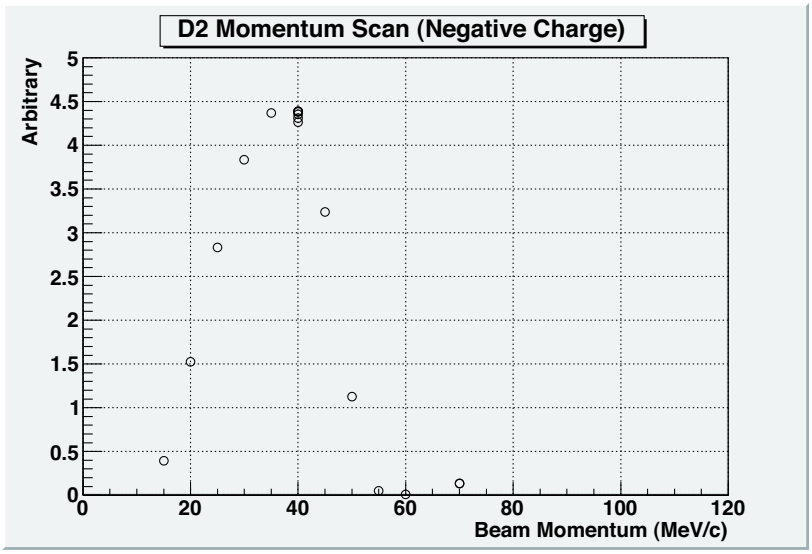

Figure 6: Momentum spectrum of the beam electron obtained by scanning the momentum setting of the beamline. A 6-mm^t Lead absorber was placed in front of counters to absorbe beam muons.

4.2.2 Pulse Kicker

The number of particles in a single burst of pulses is estimated to be 50M. Therefore, the pulse kicker is indispensable to suppress this burst of the prompt beam particles in order to protect the electron spectrometer.

Assuming that the solid angle of the beamline to be 150 msr and the size of μ-e source to be 35-mm radius, the beam emittance is 7700π mm·mrad for both vertical and horizontal. The kicker system should accept such a beam size while it is off, and block it while it is on.

Although the detailed design of the kicker system dedicated for this experiment has not been done, the feasibility of the kicker system can be established by referring to existing systems. One good example exists in the development of kicker magnet system of the RCS in J-PARC. Table 4 shows specifications of the kicker magnet system of the RCS in J-PARC. The aperture size of the RCS kicker (L type) is 10000π mm·mrad for vertical and 20000π mm·mrad for horizontal, and these are wide enough to accept the electron beam. If the electron beam entering the kicker aperture is shaped so that the horizontal size is $\pm$140 mm, the horizontal angle acceptance is $\pm$55 mrad. Therefore, in order to kick-off the beam completely, the kick angle by the kicker should be larger than 110 mrad. On the other hand, the kick angle of the kicker (L type) is 67 mrad. This is slightly less than the requirement, but the difference is only 40%. It shall be possible to develop the new kicker system which provides 60% higher performance than existing magnets. If necessary, it is also possible to use two kickers sequentially. It may need to insert a focusing element in between two kickers but that is a matter of beam optics design. Since kicker should be off when the delayed electrons are passing through it. it can be treated as a simple drift space

for the particles we are interested in. The uniformity of the magnetic field is not required, and that should make the design of kicker much easier.

The repetition rate of the kicker required is 25Hz, which is the frequency of operation of the existing kicker example. Therefore, the architecture of the power supply can be the same: using a Thyratron for the switching and PFN for the pulse forming. The fall time of the kicker should be smaller than the μ^- lifetime in Aluminum (880 nsec). The current fall time (550 nsec) is a bit larger, but still acceptable. Since the rise time can be much longer in our case, it would be possible to optimize the system to reduce the fall time at the cost of increasing the rise time.

In conclusion, the requirement for the kicker system is about the same level as that already achieved for the RCS in J-PARC. Although it is necessary to adjust the system parameters to fit the experiment, there are no serious impediments to developing the kicker system.

4.3 Electron Spectrometer

Even if the beamline it set at the 105 MeV/c momentum, there will be many particles emerging out of the beam line with other momenta. These are from DIO where the muons stop somewhere in middle of the beam line. In order to reject those off-momentum electrons, an electron spectrometer should be installed at the downstream of beam line exit. The electron spectrometer will provide a measurement the high momentum tail of DIO spectrum simultaneously, which is very important to understanding the DIO background.

The momentum resolution should be less than 1% (rms) in order to separate the μ-e electrons from the DIO electrons. The spectrometer can be a simple magnetic spectrometer with a dipole magnet and several planner tracking chambers, for example. A hodoscope and time-of-flight counters will be needed to define the timing and to reject off-timing muon backgrounds. It is also under consideration to use a large

Table 4: Specifications of kicker magnet system of the RCS in J-PARC.[19]

Dimension	Vertical	960 mm		
	Horizontal	776 mm		
	Length	638 mm		
Aperture size	Vertical	153 mm(S)	173 mm(M)	199 mm(L)
	Horizontal	280 mm		
	Length	630 mm		
B_y		480 gauss	430 gauss	370 gauss
Maximum repetition rate		25Hz		
Flat top		890 ns		
Rise time		330 ns		
Fall time		550 ns		

single NaI(Tl) crystal as in the PIENU experiment at TRIUMF.

5 Sensitivity and Background

5.1 Physics Sensitivity

Table 5 summarizes the potential sensitivity of each configuration. It is noteworthy

Table 5: Breakdown of physics sensitivity for tree configurations.

	Configuration		
	A	B	C
Muon Stopper Material	Al	Al	C
Muon Stopper Thickness	$1 \sim 3$ mm	$1 \sim 3$ mm	20 mm
Muonic Atom Rate (/sec/MW)	$(1.5 \sim 4.5) \times 10^9$	$(1.5 \sim 4.5) \times 10^9$	8×10^9
Muon Capture Rate ($\times 10^6\,\mathrm{s}^{-1}$)	0.68	0.68	0.039
μ^- life time	0.88 μs	0.88 μs	2.0 μs
Muon Capture Fraction	0.60	0.60	0.08
DIO @ 100 MeV (/MeV)	0.358×10^{-12}	0.358×10^{-12}	0.973×10^{-13}
$\mathrm{N_{DIO}}$ $E_e > 99$ MeV	9×10^{-13}	9×10^{-13}	2.4×10^{-13}
$\mathrm{N_{DIO}}$ $E_e > 101$ MeV	8×10^{-14}	8×10^{-14}	2×10^{-14}
$\mathrm{N_{DIO}}$ $E_e > 102.5$ MeV	4.7×10^{-15}	4.7×10^{-15}	1.3×10^{-15}
μ-e Relative Strength	1	1	0.7
Beamline Geom. Acceptance	150 msr	40 msr	40 msr
Time Window Acceptance	0.40 ($E_e > 102.5$ MeV)	0.40 ($E_e > 102.5$ MeV)	0.66 ($E_e > 99$ MeV)
S.E.S	$< 10^{-14}$	2×10^{-13}	8×10^{-13}

that the configuration A provides the best sensitivity.

5.2 Background

The most dangerous source of background is the prompt electron coming from off-timing protons. According to the beam test we performed, the number of prompt beam particles with 105 MeV/c is about 7×10^{-8} per proton on the muon production target for the existing beam line. The fraction of electrons in the prompt beam was only 1% and the number of prompt electrons was about 7×10^{-10} per proton. It will be 4×10^{-9} per proton for the configuration A. Therefore, the total number of off-timing protons should be less than 2×10^8 to suppress the prompt electron background. Since the total number of primary protons will be 4×10^{22} for the configuration A, the ratio between the off-timing protons to the on-timing protons, $R_{\mathrm{extinction}}$ should be less than 5×10^{-15}.

A quick beam test showed $R_{\rm extinction} < 10^{-7}$, limited by the statistics and detector's electron momentum resolution. The exact value of $R_{\rm extinction}$ is still unknown. Even if it is not 5×10^{-15} from the beginning, there is several ways to improve it. For example, the falling time of RCS extraction kickers can be improved by the modification of kicker power supply. It would also be possible to scrape the halo of proton beam before the extraction so that whole the beam shall be extracted at once. The detailed design and study with accelerator specialists of J-PARC is needed.

There are other potential backgrounds those have to be evaluated such as cosmic-ray induced backgrounds, sky-shine neutron induced backgrounds, delayed neutron induced backgrounds where the neutrons are coming back from the neutron target. Although, these will be studied for the proposal, let us comment on the cosmic-ray induced background. Since the duty factor of the detector live time for this experiment is only an order of 10^{-4}, the effect of the cosmic-ray induced background to this experiment is 10^{-4} times less than COMET/Mu2e type experiment. In addition, the sensitivity goal is two orders of magnitudes larger than COMET/Mu2e. Therefore, the cosmic-ray induced backgrounds will be very small.

6 Schedule and Cost

Although the physics sensitivity of this experiment is two orders of magnitude less than the goals of COMET and/or Mu2e, it has three potential advantages, namely simplicity, schedule, and cost.

This experiment would need one year to finalize the overall design. Once the construction has began, procuring magnets and the kicker could be accomplished in two years or less. With two years of data taking it is quite promising to have a first result within five years form now if there were no impediments due to funding.

As for the cost, the axial focusing magnet for the new beam line would be $2 \sim 3$ Oku-Yen, the kicker system 2 Oku-Yen, and the detector system would be less than 1 Oku-Yen. These three components should be newly built. Other beamline magnets may be procured from other institutes such as TRIUMF. The radiation shield may need several Oku-Yen, but the shield is also necessary for any future projects in the Muon Facility.

7 Summary

The muonic atom formation rate in an Aluminum disk placed nearby the Muon Target in MLF is quite high, a few times 10^9/sec/MW. Therefore, the experiment searching for μ-e conversion at a level of 10^{-14} is feasible if a large-acceptance high-momentum electron beamline is built at the High-Momentum Decay Muon port.

The whole idea of this experiment is suited for the MLF J-PARC since it utilizes special features of the proton beam at MLF:

- Pulsed time structure to suppress background; and

- High power to increase sensitivity.

Therefore, the authors are very interested in realizing the experiment at the High-Momentum Decay Muon port at MLF Muon Facility.

The cost of this experiment may be only one tenth or less that of COMET/Mu2e and physics results can be obtained well before these projects, perhaps leading to a major new discovery in fundamental particle physics.

Detailed design work of the experiment is on-going. Several beam tests were performed at D2 to understand the muonic atom formation rate as well as proton extinction level. A proposal will be submitted in timely manner.

References

[1] V. Barger, D. Marfatia and K. Whisnant, Int. Jour. Mod. Phys. E **12** 569 (2003).

[2] A. de Gouvêa, in *NEUTRINO FACTORIES AND SUPERBEAMS, 5th International Workshop on Neutrino Factories and Superbeams, NuFact03*, edited by A. Para (American Institute of Physics, Melville, New York), p. 275 (2004).

[3] M.L. Brooks *et al.* (MEGA Collaboration), Phys. Rev. Lett **83** 1521 (1999).

[4] U. Bellgardt *et al.*, Nucl. Phys. B **229** 1 (1988).

[5] P. Wintz *et al.*, in *Proceedings of the First International Symposium on Lepton and Baryon Number Violation*, edited by H.V. Klapdor-Kleingrothaus and I.V. Krivosheina, (Institute of Physics Publishing, Bristol and Philadelphia), p.534, unpublished (1988).

[6] W. Burtl *et al.* (The SINDRUM II Collaboration), Eur. Phys. J. C **47** 337 (2006).

[7] J. Hisano *et al.*, Phys. Lett. B **391** 341 (1997); **397** 357(E).

[8] J. Hisano *et al.*, Phys. Rev. D **58** 116010 (1998).

[9] J. Hisano and D. Nomura, Phys. Rev. D **59** 116005 (1999).

[10] F. Borzumati and A. Masiero, Phys. Rev. Lett. **57** 961 (1986).

[11] R. Barbieri and L.J. Hall, Phys. Lett. B **338** 212 (1994).

[12] R. Barbieri *et al.*, Nucl. Phys. B **445** 219 (1995).

[13] K. Ishida, *private communication.*

[14] O. Shanker, Phys. Rev. D **25** 1847 (1982).

[15] P.A. Piroue and A.J.S. Smith, Phys. Rev. **148** 1315 (1966).

[16] M.G. Catanesi *et al.*, Eur. Phys. J. C 53, 177–204 (2008).

[17] N.T. Zinner, K. Langanke and P. Vogel, arXiv:nucl-th **0606002** (2006).

[18] R. Kitano, M. Koike and Y. Okada, Phys. Rev. D **66** 096002 (2002).

[19] J. Kamiya *et al.*, *Proceedings of the 19th International Conference of Magnet Technology*, Genova, Italy, 18–23 September 2005, MOM3OR3.

[20] A. Aguilar-Arevalo *et al.*, N.I.M. A **609** 102 (2009).